

This work is on a Creative Commons Attribution-NonCommercial-NoDerivatives 4.0 International (CC BY-NC-ND 4.0) license, <https://creativecommons.org/licenses/by-nc-nd/4.0/>. Access to this work was provided by the University of Maryland, Baltimore County (UMBC) ScholarWorks@UMBC digital repository on the Maryland Shared Open Access (MD-SOAR) platform.

Please provide feedback

Please support the ScholarWorks@UMBC repository by emailing scholarworks-group@umbc.edu and telling us what having access to this work means to you and why it's important to you. Thank you.



Microtensile characterization of titanium 5111 alloy mechanical properties and comparison of failure mechanisms at two microstructural length scales

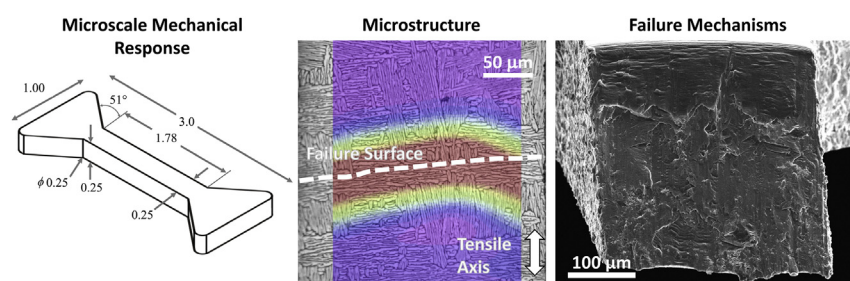
Salahudin Nimer¹, Richard K. Everett^{*}, Marc Zupan

University of Maryland Baltimore County, 1000 Hilltop Circle, Baltimore, MD 21250, United States of America

HIGHLIGHTS

- Novel use of microtensile testing and strain contour mapping relates failure location to microstructure.
- Base metal exhibits large variations in strength due to large colony structures.
- Friction stir welded stir zone metal exhibits a refined grain structure and higher, more uniform strengths.

GRAPHICAL ABSTRACT



ARTICLE INFO

Article history:

Received 30 May 2019

Received in revised form

16 July 2019

Accepted 27 July 2019

Available online 29 July 2019

Keywords:

Titanium alloys

Mechanical testing

Microstructure

Friction stir welding

ABSTRACT

Micro-scale mechanical characterization of materials is a useful technique for understanding local material behavior, particularly where inhomogeneous materials or microstructures are present. In this work, a custom microsample testing system that utilizes digital image correlation (DIC) is used to measure the response of samples that have a $3\text{ mm} \times 1\text{ mm}$ footprint and a cross sectional gage area of $250\text{ }\mu\text{m} \times 250\text{ }\mu\text{m}$. The mechanical behaviors of Ti-5111 base metal and friction stir weld refined microstructures were examined. In a novel use of strain contour mapping, microstructural analysis and measurements were performed directly on microsamples and these results were linked to the fractography and measured properties using the DIC data. Larger variations, in several mechanical properties, were measured in the base metal Ti-5111 than in the weld material. For example, the yield base metal stress was $771 \pm 41\text{ MPa}$ versus $828 \pm 9\text{ MPa}$ for the weld. These variations were found to be due to the larger colony structure of the wrought plate. The colonies in wrought plate Ti-5111 can be as large as $250\text{ }\mu\text{m}$ and were found to promote the formation of shear bands which resulted in reduced ductility.

© 2019 The Authors. Published by Elsevier Ltd. This is an open access article under the CC BY-NC-ND license (<http://creativecommons.org/licenses/by-nc-nd/4.0/>).

1. Introduction

Ti-5111 (Ti-5Al-1Sn-1Zr-1V-0.8Mo wt%) is a near- α titanium alloy that was developed as a lower cost alternative to Ti-100 (Ti-5Al-2Nb-

1Ta-0.8Mo) with increased fracture toughness and corrosion resistance than Ti-6Al-4V. This makes Ti-5111 an attractive material for use in naval and other marine-environment applications.

The ability to measure local material properties is particularly important where inhomogeneous materials or microstructures are present, or when a limited volume of material is available. Recent work has used a microsample tensile testing approach to characterize the location- and orientation-specific mechanical properties of friction stir welded Ti-5111 [1,2]. Microsample characterization was conducted to document the specific microstructural regions within

^{*} Corresponding author.

E-mail address: salahudin.nimer@jhuapl.edu (S. Nimer), rick.everett@umbc.edu (R.K. Everett), mzupan@umbc.edu (M. Zupan).

¹ Present Address: The Johns Hopkins University Applied Physics Lab, 11100 Johns Hopkins Road, Laurel, MD 20723

the weld, as well as spanning the interphase between the weld and the base metal.

The properties of ductile materials can be greatly affected by the number of grains or phases present within the microsample gage section, as well as their orientations. In typical macrosample tensile tests there are many grains contained within the gage section and some average mechanical behavior is measured. In microsample tests, this averaging may not be possible simply due to fewer grains in the gage section and limited occurrences of orientations. One way to ensure there are sufficient grains in a microsample is to interrogate a very fine, equiaxed microstructure. For titanium alloys, these exact refined microstructures occur in the stir zones of friction-stir welded or processed materials. In this paper, we compare the microtensile behavior of Ti-5111 which exhibited two different microstructures: wrought plate base metal (BM) and the stir zone of a friction stir weld (FSW). Any differences (beyond Hall-Petch type hardening) should reflect local microstructure-property mechanisms and relationships. This local characterization provides valuable grain-scale information that is otherwise unavailable or masked by the usual macro-scale characterization methods.

An important aspect of microsample testing is the selection of an accurate method to measure strain. The microsample geometry used in this work has been previously used to characterize a variety of materials [1–6]. Due to the limited dimensions of the samples, non-contact strain measurement methods must be used. Recently, digital image correlation (DIC) techniques [7,8] have been employed [9,10]. DIC measures surface strains by tracking the movement and deformation of distinct subregions mapped between sequential digital images captured while loading the body containing the surface. Distinct regions may be recognized from surface features inherent to the sample, or more usually, by placing a random speckle pattern on the sample surface. DIC has been used to track macroscale [11] and microscale [12,13] strains, dynamic strains [14], and even biomaterial strains [15]. The primary advantages of using DIC are the abilities to obtain full field deformations and measure larger strains.

A custom microsample testing system, that utilizes DIC to measure strain responses, provides micro-scale measurements of the elastic modulus, yield strength, ultimate tensile strength and strain to failure. Data are compared to previous studies [1,2,5] of the micro-scale behavior of specific weld regions of FSW and BM Ti-5111. DIC analyses were used to generate full-field strain contour maps that were superimposed over the undeformed microstructures of the individual microsamples to reveal important performance-controlling features and failure mechanisms. The use of micro-scale tensile testing is a sensitive new tool for evaluating microstructure-specific mechanical properties and localized failure mechanisms.

2. Materials & methods

2.1. Materials

The 12.7 mm thick wrought plate of Ti-5111 was provided by the Naval Surface Warfare Center, Carderock Division. The friction stir welding was performed by the Edison Welding Institute. Butt welds were fabricated at 200 rpm spindle speed, and a tool travel of 1.48 mm s^{-1} under argon shielding gas. The pin tool was a tungsten-based pin, with a smooth tapered 7.62 mm head. The reader is directed to reference [6] for further details on the bulk properties of Ti-5111 and on the processing of the weld. Information on friction stir welding of titanium alloys may be found in reference [16].

2.2. Characterization & mechanical testing

Micro-tensile specimens were prepared in a similar manner for each (BM & FSW) material. To prepare the microtensile specimens, the plate is first sectioned into a 1 mm thick slice using a Fanuc Robocut Alpha OiE wire electrical discharge machining (EDM) process. Microsamples were extracted from the slice using a custom finishing pass setting with a 0.25 mm diameter wire which results in a slow, controlled cut which reduces the damage to the material [5]. EDM was carried out such that the tensile axis was along the transverse rolling direction (TD) in order to match the orientation of the macro-sized specimens from literature. Fig. 1 shows the microsample geometry and the approximate sampling locations within the plate. The total microsample footprint is $1 \text{ mm} \times 3 \text{ mm}$ with a final gage area of $250 \mu\text{m} \times 250 \mu\text{m}$. After machining, the sample surfaces were prepared using 180, 320, 400, 600, 800 and 1200 grit SiC papers. Samples were finished with a vibratory polish using a 10:1 mixture of $0.04 \mu\text{m}$ colloidal silica and 30% hydrogen peroxide. The samples were then etched using Kroll's reagent.

Microstructural measurements on prepared microsamples were made on an Olympus BX51 optical microscope. Due to the refined structure of the Ti-5111 FSW, an FEI Nova NanoSEM 450 was used for microstructural analysis of the weld samples. For each sample, the average α lath thickness, average prior β grain size, and average α colony size were measured directly from the microsamples. Both the average prior β grain size, and average α colony size were measured using a linear intercept method using randomly placed lines [17]. The α lath thickness was measured by first thresholding all images and then using commercial software (Fovea Pro) to calculate the mean lath thickness [18].

A high contrast speckle pattern, with spots of appropriate size ($3.4 \mu\text{m}$ average diameter) and 1:1 coverage of white to black for sufficient resolution, was applied to the microsamples in order to measure in-plane strains via DIC. Black paint speckles were applied with an airbrush (Rust-Oleum high heat enamel diluted with acetone

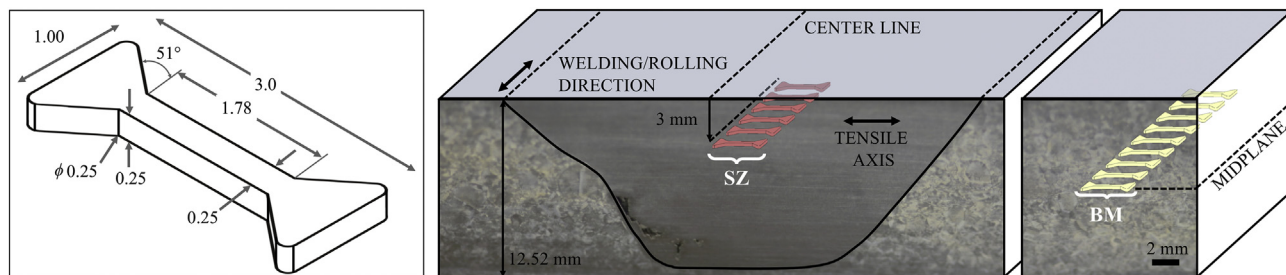


Fig. 1. Microtensile sample schematic with dimensions (in millimeters) and sample locations in the Ti-5111 plate.

in a 1:1 ratio by weight) over white-painted microsamples. Images were acquired with a Guppy Pro F-146 camera providing 1.4 megapixels (MP) at a rate of 4 frames per second, outfitted with a Navitar 12× Ultrazoom lens. This resulted in a resolution of approximately 0.5 pixels/ μm^2 . The DIC analyses were conducted using commercially available software (VIC-2D by Correlated Solutions). The subset size was set to 31–45 pixels, based on the size of the speckles. This resulted in ≈ 3 –4 speckles within a subset. A step size of approximately one-quarter of the subset size was used. The spatial resolution is related to the subset and step size [19,20]. For the chosen parameters, a spatial resolution of between 5 and 30 μm was achieved, which assuming uniform strain translates to a strain resolution of approximately 1%. This resolution is sufficient to accurately determine the strain localization within colonies and achieve strain maps with no gaps in the field.

Select DIC analyses were used to generate strain contour maps that were then superimposed over undeformed microstructural images of the microsamples. In order to measure displacements and strains, DIC

uses deforming subsets to track the unique speckles contained in each subset. At the end of the mechanical test, the deformed and displaced DIC subsets were digitally enhanced by the DIC software with a gradient color scale corresponding to the amount of strain within each subset. VIC-2D allows for visualization of an “un-deformed” image which shows the change in strain within the original position and size of each subset. This visualization can then be manually aligned and overlaid on the microstructural image using the undeformed grip section of the microsample as an alignment guide. These strain maps thus reveal the eventual strain localizations within these microstructures.

The microsamples were tested on a custom microsample load frame designed to meet the challenges of testing micromechanical specimens. The load frame used a piezoelectric actuator, and all samples were tested at a quasi-static strain rate of 10^{-4} s^{-1} . The load cell used for all microsample experiments provided a resolution of 0.0022 N. A National Instruments USB-6211 multifunction I/O device was used to acquire load voltage signals. A linear air

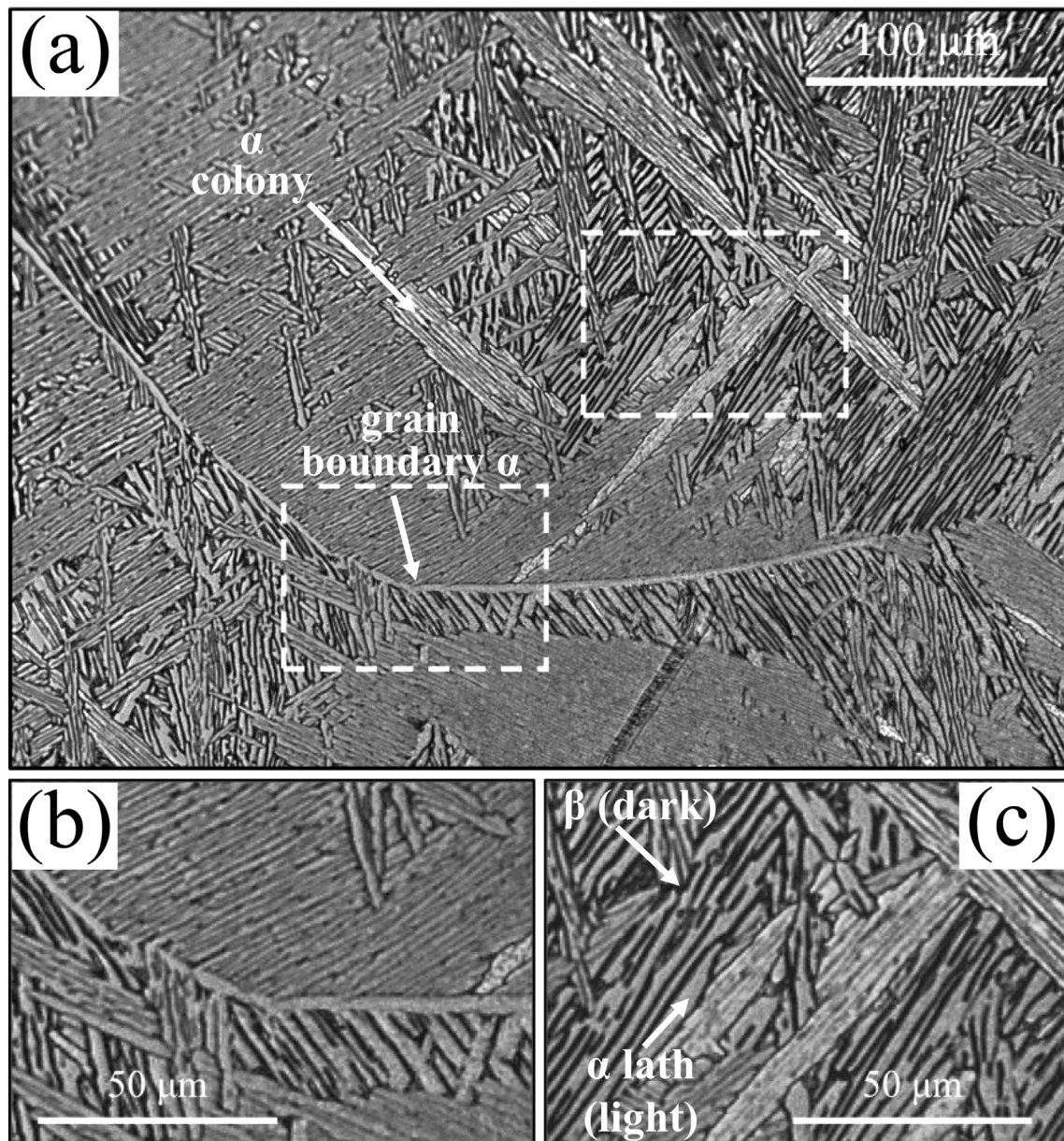


Fig. 2. Microstructure of base metal Ti-5111 in the ST-TD. Inset boxes in (a) correspond to magnified regions shown in (b) and (c).

Table 1
Summary of average measured Ti5111 TD-RD microstructural features.

| Material | Prior β grain size (μm) n = 100 | Colony Size (μm) n = 100 | α lath thickness/ α diameter (μm) n = 1000 |
|----------------|---|--|---|
| Ti-5111 BM | >1000 | 33 ± 45 | 0.81 ± 0.07 |
| Ti-5111 FSW SZ | 33 ± 11 | 10 ± 8 | 0.13 ± 0.01 |

bearing was used to minimize any friction during the test. More information of the testing system may be found in Reference [5]. All fracture surface images presented were obtained using an FEI Nova NanoSEM 450. Fovea Pro was also used to measure void size on select fracture surfaces.

3. Results

3.1. Microstructure of base metal Ti5111

The base metal Ti-5111 examined in this work, and shown in Fig. 2, consisted of prior β grains larger than 1 mm. This is consistent with other literature values [21]. The short transverse-rolling direction (ST-RD) orientation was used to analyze the microstructure within the sample cross sectional area ($250 \times 250 \mu\text{m}$), and the transverse direction-rolling direction (TD-RD) orientation was used to analyze the microstructure within the microsample width and length ($\sim 1.8 \text{ mm}$). Table 1 presents a summary of the BM TD-RD microstructure measurements. The ST-RD orientation average colony size was $21.3 \pm 25 \mu\text{m}$. It is difficult to definitively measure the prior β grain size due to the fact that the processing of the rolled plate resulted in a microstructure with discontinuous grain boundary α . Multiple prior β grains were likely present within the length of each microsample, as shown in Fig. 3a. Although the grain boundary is prominent in Fig. 3a, it likely did not continue all the

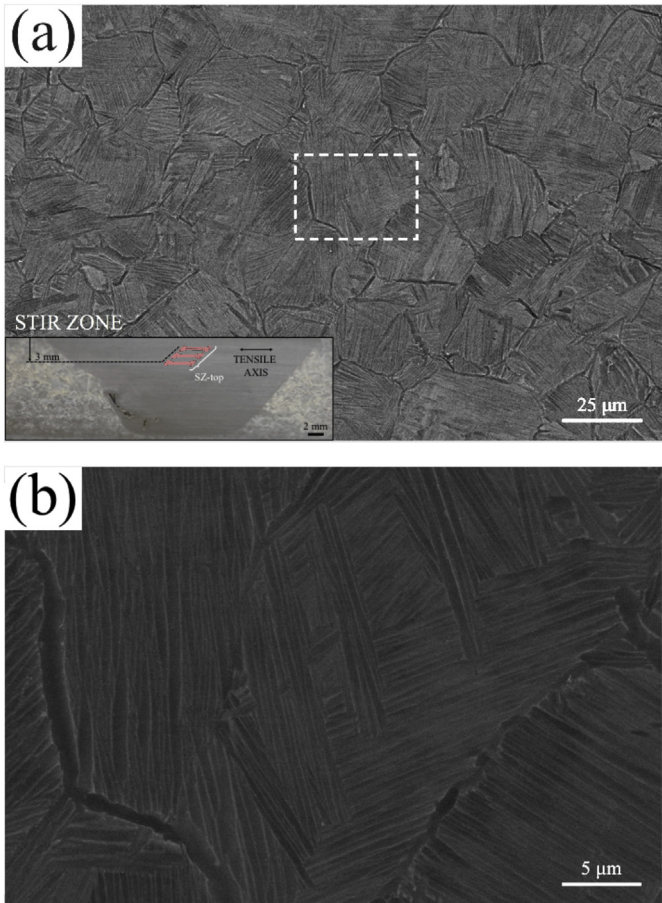


Fig. 4. Microstructure of Ti-5111 SZ in the TD-RD. Higher magnification image in (b) corresponds to the boxed region in (a).

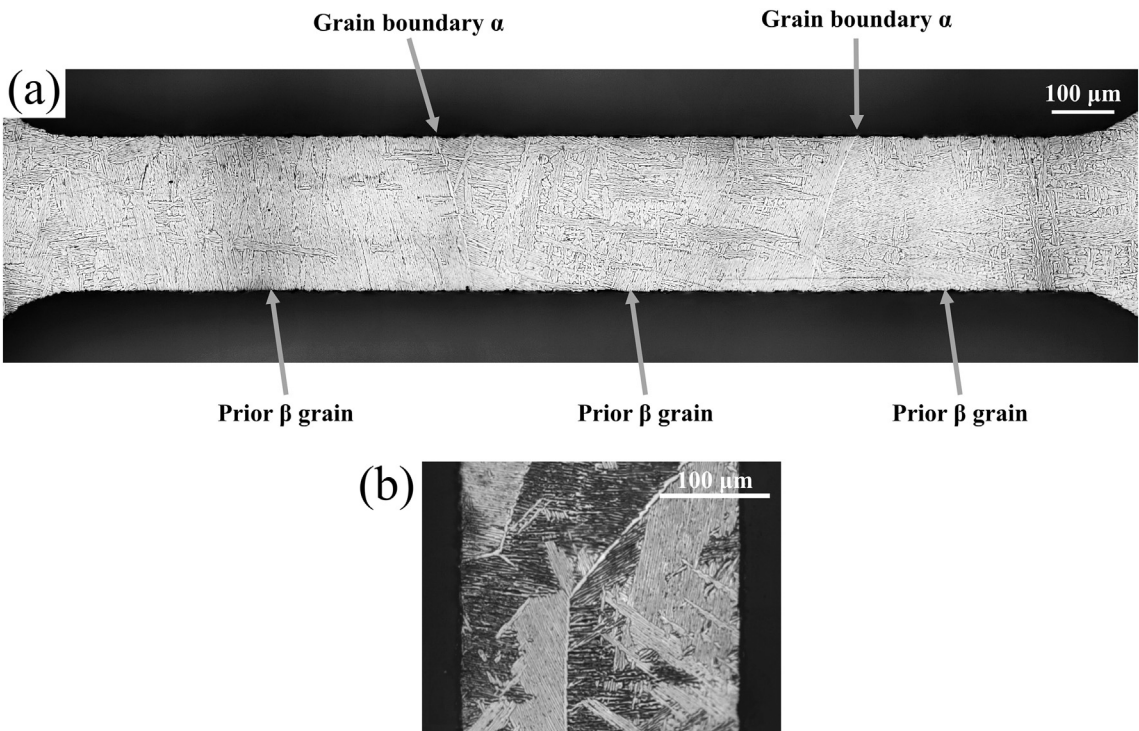


Fig. 3. Ti-5111 BM microstructure within microsample showing prior β grains with α decorating the grain boundary. a) TD-RD. b) ST-RD.

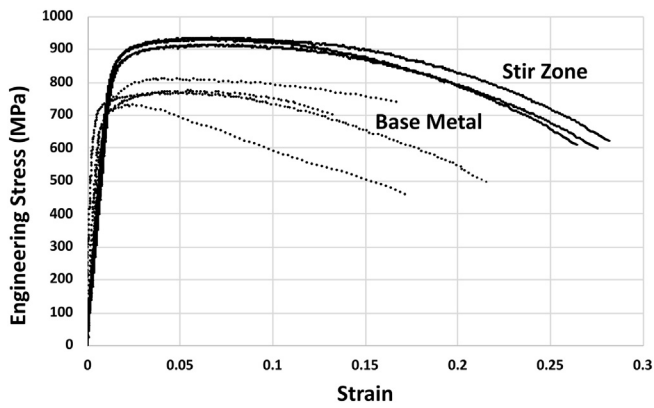


Fig. 5. Typical stress-strain responses of base metal (dashed lines) and stir zone (solid lines) Ti-5111 microtensile samples.

way through the thickness of the sample due to the fact that for all samples examined in this work, failure at grain boundary α was never observed. Failure at grain boundary α is common in cast Ti-5111 with a continuous network of grain boundary α [22].

3.2. Microstructure of FSW Ti5111

The FSW process typically produces a narrow (≈ 500 mm) thermomechanically affect zone separating the BM from the SZ [21]. The SZ exhibits a relatively equiaxed microstructure with refined α laths

within equiaxed prior β grains as shown in Fig. 4. All microsamples were extracted from the midplane of the wrought and welded plate. The microstructural feature measurements of the stir zone (SZ) are also presented in Table 1. These measurements are in agreement with previously published values for FSW Ti-5111 welded under similar conditions [2].

3.3. Mechanical testing BM Ti-5111

Fig. 5 shows the stress strain responses of select base metal Ti-5111 microsamples. Since macro-samples average over many grains, to compare the location-specific properties to literature values we consider pooling the results and presenting the averages. The measured average micro-scale elastic modulus, yield strength, and ultimate tensile strength agreed with literature values as shown in Table 2. However, the measured average micro-scale ultimate tensile value was 8% less than the macro-scale result, which may be attributed to the fact that these microsamples were extracted from the middle of the plate. The middle of the plate experiences the least amount of deformation.

during the rolling process, and macro-sized tension test samples are typically harvested from the plate such that the gage volume captures the free surfaces that contain stronger, more deformed material. This may explain the slight difference in ultimate tensile strength between the base metal macro-scale value and the microsample measurement. The lowest measured strain to failure was 6.5%, which is similar to the minimum value of 10% set by ASTM Grade Standards. Although the average measured strain to failure

Table 2
Summary of average (\pm standard deviation) BM-Ti-5111 microsample transverse direction (TD) properties.

| Property | BM microsample measurement (n = 9) | Macroscale literature | SZ microsample measurement (n = 6) | ASTM B265 grade 32 |
|--------------------------|------------------------------------|-----------------------|------------------------------------|--------------------|
| E (GPa) | 110 \pm 23 | 107–114 [23] | 69 \pm 6.9 | |
| σ_Y (MPa) | 771 \pm 41 | 780 \pm 27 [23,24] | 828 \pm 9 | 590 (min.) |
| σ_{UTS} (MPa) | 799 \pm 39 | 869 \pm 14 [23,24] | 930 \pm 9 | 690 (min.) |
| $\epsilon_{failure}(\%)$ | 14 \pm 6.3 | 14 \pm 1.5 [23,24] | 27.4 \pm 0.75 | 10 (min.) |

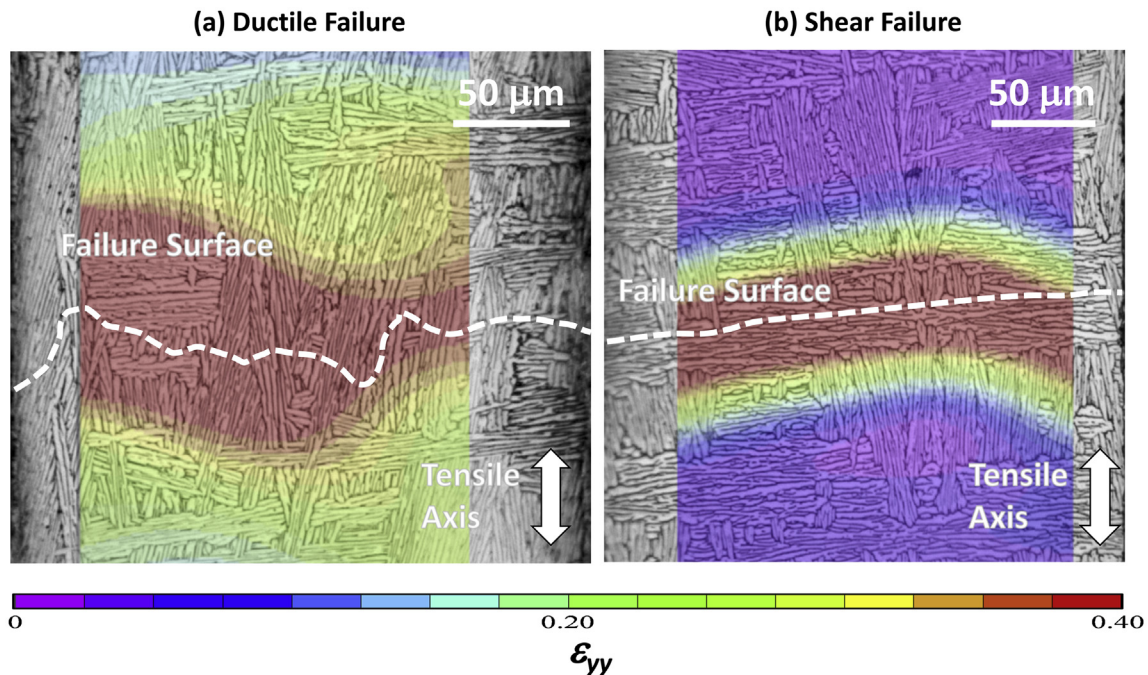


Fig. 6. DIC analysis of final ϵ_{yy} strain overlaid on initial microstructure of base metal Ti-5111 microsamples showing localization within the microstructures of a typical (a) ductile failure and (b) shear failure. The approximate locations of the failure surfaces are shown with dashed lines.

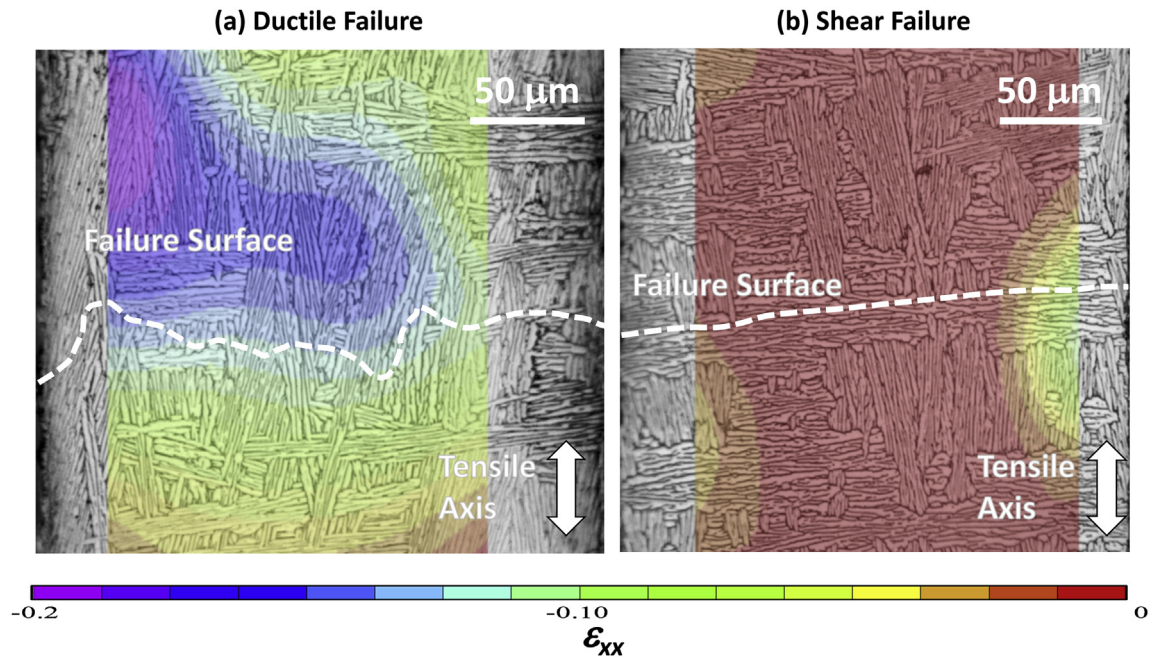


Fig. 7. DIC analysis of final ϵ_{xx} strain overlaid on initial microstructure of base metal Ti-5111 microsamples showing localization within the microstructures of a typical (a) ductile failure and (b) shear failure. The approximate locations of the failure surfaces are shown with dashed lines.

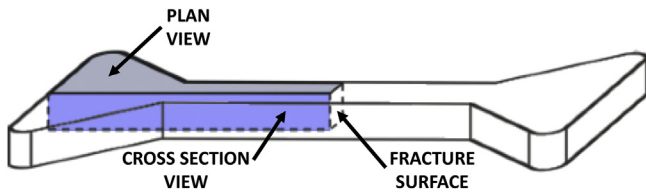


Fig. 8. Schematic of the microsample showing locations of the polished and etched cross section and plan views in relation to the fracture surface.

agrees with literature, the standard deviation is much higher than what occurs at the macro scale, and higher than that observed for the refined stir zone microstructure.

Pooling the data allows the computation of the sample standard deviation and a quantification of local property variation. The large standard deviation in strain to failure (compared to literature values) was found to be due to two distinct failure modes that occur, corresponding to the measured ductility of the samples. The lower strain to failure samples fractured under shear rupture with

shear dimples present on the fracture surface. The failure surface of all these samples was measured to be at a 45° angle to the tensile axis. The higher strain to failure samples exhibited ductile rupture with necking and microvoid coalescence on the fracture surface. The mean strain to failure for the shear versus ductile failure modes was a statistically-significant ($p = 0.05$) difference of 10.7 ± 3.8 versus $20.6 \pm 6.6\%$.

The microstructures of the samples in the strain localization region corresponding to the two failure modes were analyzed in order to relate the local microstructure to the failure mechanisms. DIC strain contour maps were overlaid onto the microstructural images, showing the location of ϵ_{yy} (in the tensile direction; Fig. 6) and ϵ_{xx} (perpendicular to the tensile direction; Fig. 7) strain localization within the microstructure. The eventual position of the failure surface is also marked. In ductile failures (Figs. 6a and 7a), the strain diffusely localized in a grouping of α colonies which were mainly oriented parallel to the tensile axis. This allowed strain to distribute among the laths leading to the laths elongating, contributing to the larger strain to failure. This is very different

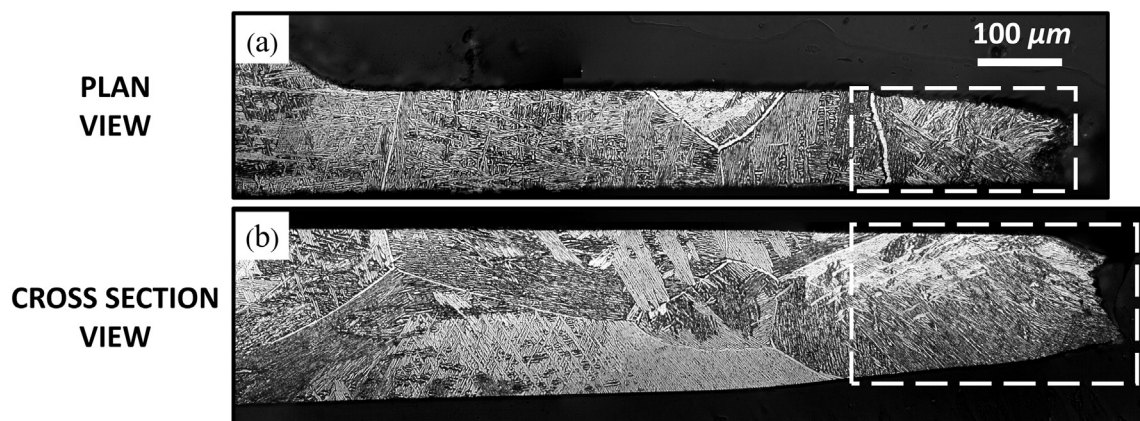


Fig. 9. Plan view (a) and cross section view (b) of a polished and etched BM microtensile sample with higher ductility ($\epsilon_f = 26.4\%$). Regions indicated in (a and b) correspond to enlarged images shown in Fig. 11.

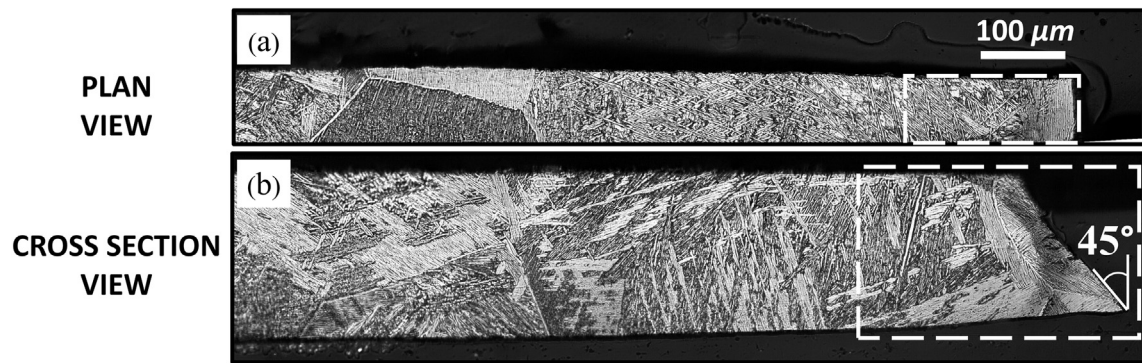


Fig. 10. Plan view (a) and cross section view (b) of a polished and etched BM microtensile sample with lower ductility ($\epsilon_f = 13.2\%$). Regions indicated in (a and b) correspond to enlarged images shown in Fig. 12. Note the 45° shear failure.

from shear failures (Figs. 6b and 7b). These samples typically localized in a single narrow α colony that was perpendicular to the tensile axis and did not neck, and as a result did not accumulate any significant ϵ_{yy} strain. Thus, strain was able to distribute throughout the colonies for the ductile fracture samples but was forced to concentrate within a smaller region for the shear failure samples.

To further investigate the internal microstructure of the samples, two additional samples were selected to examine the microstructures after testing in two planes: (1) through cross section and (2) in the plan view (see Fig. 8). Figs. 9 and 10, the higher and lower ductility samples respectively, present the microstructures in the samples, along the gauge lengths away from the fracture surfaces, which consisted mainly of colonies either oriented nearly parallel to the tensile axis or a basketweave structure, respectively. Fig. 9, of the sample with above average ductility, showed significant necking which was apparent in both the cross section and plan views. The sample that showed below average ductility, Fig. 10, however, showed very little necking and fractured at a 45° angle to the tensile axis. Figs. 11 and 12 show enlarged images of the

microstructures near the failure locations for the samples shown in Figs. 9 and 10, and how the local microstructure correlates with the fracture surface.

As indicated in Fig. 11, the sample that exhibited the higher ductility had the majority of laths oriented with the tensile axis, 16° and 23° in the cross section and plan views respectively. Fig. 11 also shows the laths deforming near the fracture surface and this corresponds to the void coalescence observed on the fracture surface in Fig. 13a. If a colony was large enough to span the entire gage cross section and was oriented such that the laths were parallel to the tensile axis, this would lead to a high strain to failure. If there were smaller colonies within the gage area and the laths were oriented parallel to the tensile axis, this would also lead to a high strain to failure.

However, in order for this to occur, there should be no unfavorably oriented laths of a large enough size throughout the gage length of the sample, which is a rare occurrence. This can be seen in the cross section of a sample that accommodated a large strain to failure, shown in Fig. 11. Throughout the gage length of the sample,

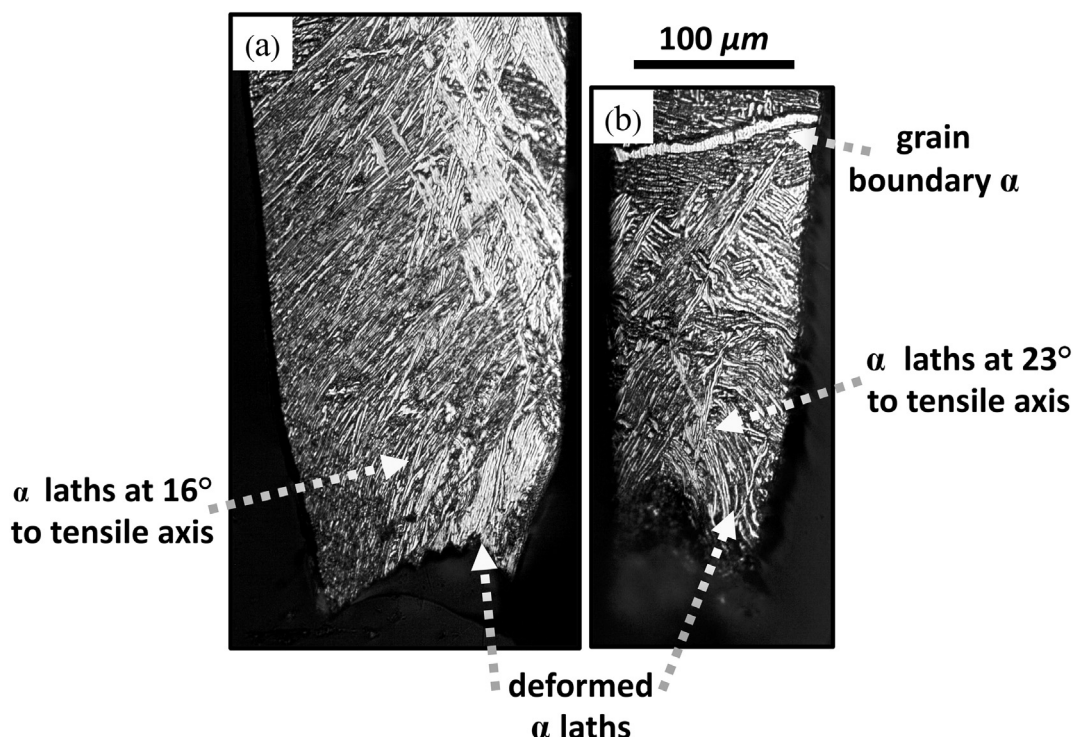


Fig. 11. Magnified regions near the fracture surface from the cross section (a) and plan (b) views as indicated in Fig. 9.

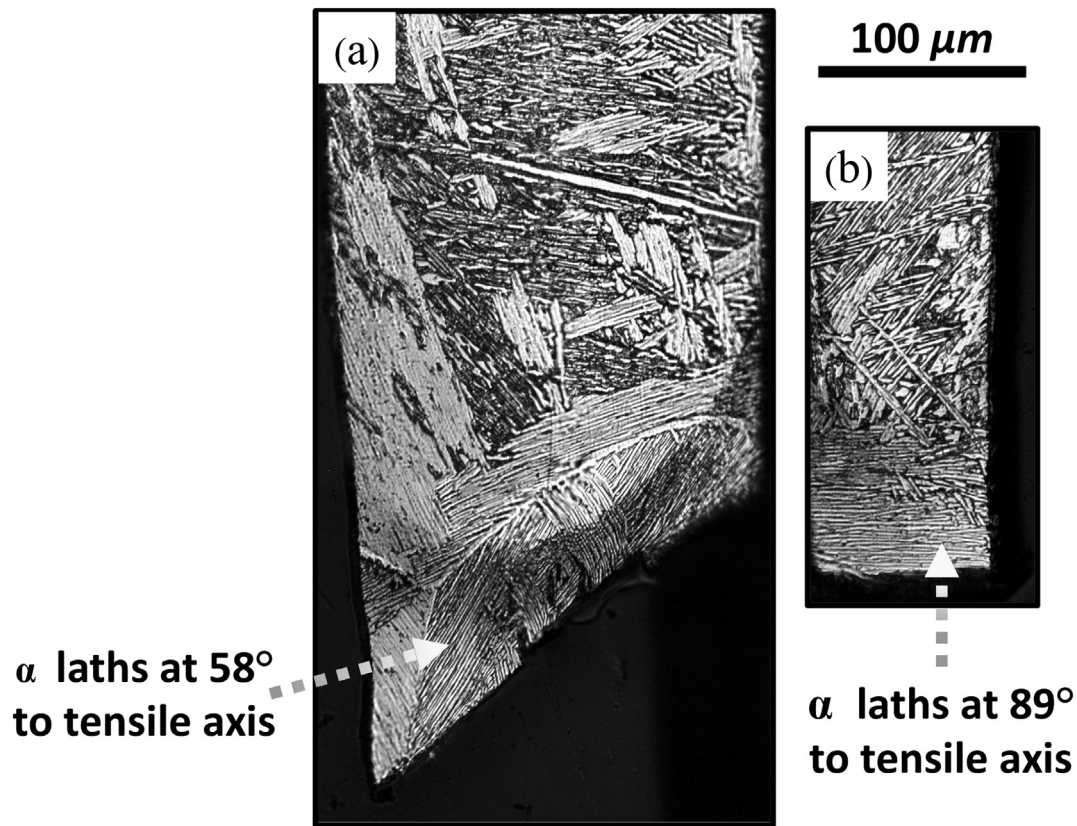


Fig. 12. Magnified regions near the fracture surface from the cross section (a) and plan (b) views as indicated in Fig. 10.

there were no areas where shear failure would be favorable, such as misoriented colonies that span the width or thickness of the sample. The probability of this occurring within the gage volume of the sample is likely rarer than the alternative, which may be the reason why shear failure was observed more often than the ductile fracture. Fig. 12 shows that with the sample that displayed the lower

ductility, in the plan view the samples were oriented nearly perpendicular to the tensile axis and within the cross section view the laths were oriented at a 58° angle to the tensile axis. This sample also fractured within a prior β grain approximately $250\ \mu\text{m}$ in diameter. It should be noted that fracture surface (Fig. 13b) occurred at a 45° angle and did not occur in between the laths. The

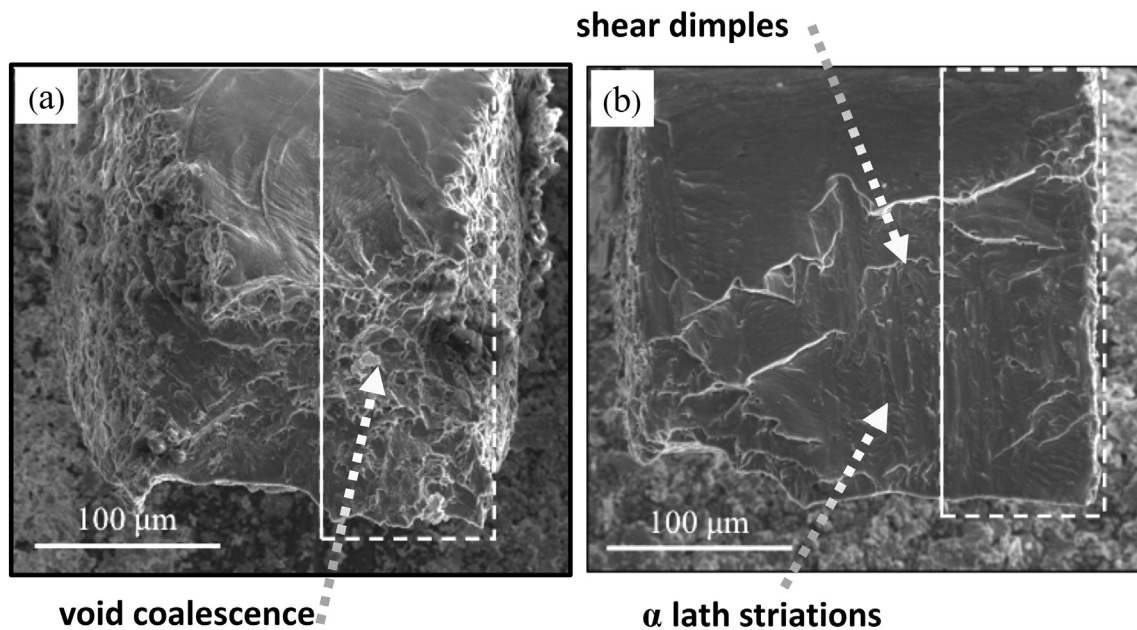


Fig. 13. Fracture surfaces of select base metal Ti-5111 microsamples that exhibited (a) ductile void coalescence with above average ductility and (b) shear fracture with below average ductility. The highlighted regions are the approximate areas which remained after polishing. The solid white lines are the approximate locations of the cross section surfaces in Figs. 9–12.

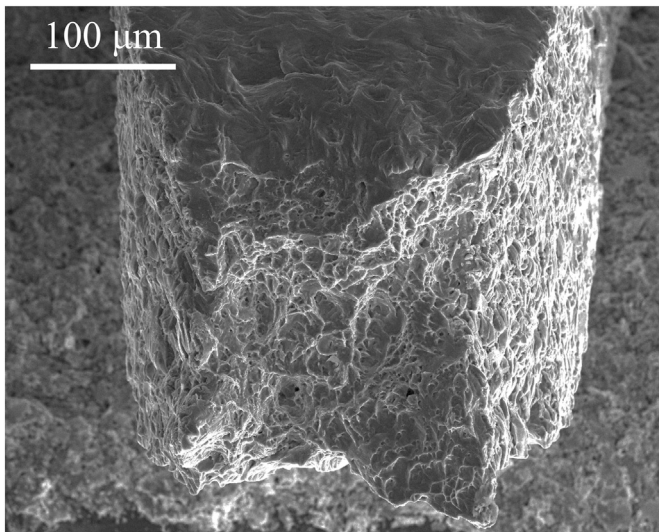


Fig. 14. Typical fracture surface of a SZ Ti-5111 microsample.

six samples that failed in this manner had an average fracture angle of $47 \pm 5^\circ$. The location where failure occurred is the only location through the gage section where a large colony that is unaligned with the tensile axis spans the entire thickness and half of the width. It is proposed that for each sample that failed by shear the failure location was decided by two conditions: (1) the relative size of the colony in three dimensions was large compared to other colonies within the gage volume and (2) the orientation of the laths inside the colonies were more misoriented with respect to the tensile axis. An analysis was conducted to measure the area of the largest colony (within a $250 \mu\text{m}$ square overlaid on the microstructure in the ST-RD view) which gives an understanding of the size of the largest possible colony that might be present within the gage section of the samples. It was found that there is a 71% probability that the sample gage length will have a colony as large as 35% of the cross section.

It is important to note that fracture did not occur along the grain boundary α present around the prior β , which is most likely due to the fact that base metal Ti-5111 displays a discontinuous grain boundary α structure, as can also be observed in Fig. 11 with grain boundary α being present in one view but not continuing to be visible in another. This variation in failure modes and ductility is a direct result of the size of microstructural features present in base metal Ti-5111 in relation to the size of the microsamples.

3.4. Mechanical testing FSW Ti-5111

Typical stress-strain curves are shown in Fig. 5, and a summary of the mechanical test data from the FSW Ti-5111 is presented in Table 2. The yield strength, ultimate tensile strength, and strain to failure for the FSW material were higher and showed significantly less variation than the BM. This is expected since the FSW process produces a microstructure with refined α laths within equiaxed prior β grains. The refined equiaxed structure meant all microstructural features were much smaller than the length scale of the microsample, and that multiple α colonies with random geometric lath orientations existed within the gage length. As a result of the more homogeneous microstructure, the strain was allowed to uniformly distribute throughout the sample and did not preferentially localize. Fig. 14 presents a typical ductile failure fracture surface from a SZ Ti-5111 microsample. The weld fracture surfaces showed microvoid coalescence. The base metal's higher standard deviation in ultimate tensile strength may be due to slight

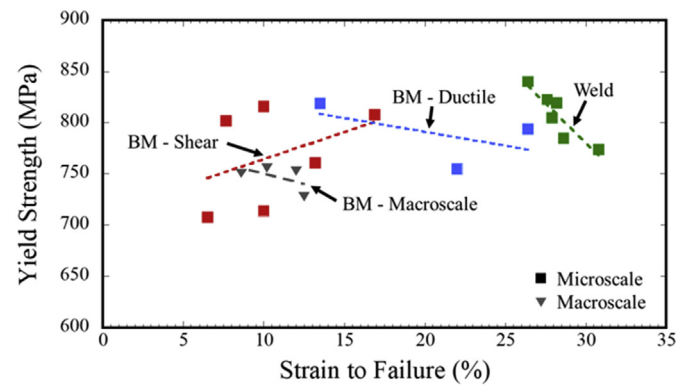


Fig. 15. Yield strength versus strain to failure for Ti-5111. Microsample measurements from the current work and macroscale literature measurements at various heat treatments are shown.

differences in local microstructure from sample to sample.

A comparison of the measured weld properties with previous work [6] indicates generally good agreement. A deviation from past results occurs in the measured strain to failure measurements, with values that are slightly greater than the literature values. This could be attributed to microstructural changes due to the difference in depth within the weld.

4. Discussion

The micro-scale mechanical properties were comparable to macro-scale measurements and previous microscale measurement for the materials examined. Previous studies [1,2] measured the average BM YS and UTS as 750 and 795 MPa, similar to the respective 771 and 799 MPa values measured in this work. Note that the previous work also documented the BM strength anisotropy measuring a longitudinal (RD) UTS of 701 MPa.

The measured BM Young's moduli are quite a bit higher than the SZ moduli, but are similar to literature values. This might indicate the presence of voids or other defects in the FSW materials.

An increase in yield strength typically corresponds with a decrease in ductility. In order to compare the responses of the measured properties in this work, the yield strength versus strain to failure for Ti-5111 is examined in Fig. 15. The microsample measurements are separated into three groups, the BM samples that failed by shear, the BM samples that failed by ductile fracture, and the weld SZ samples. Macroscale literature values for base metal Ti-5111 are also shown.

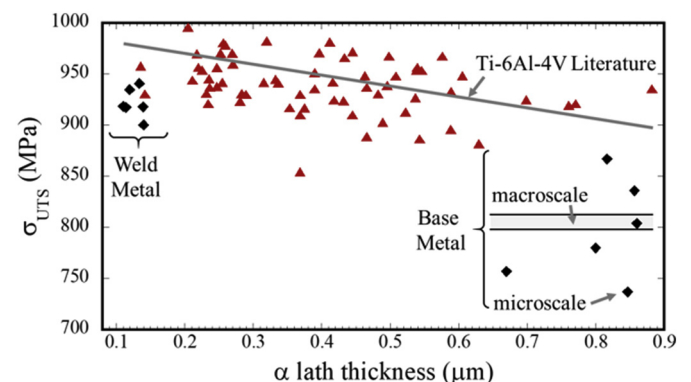


Fig. 16. Ultimate tensile strength of Ti-5111 versus α lath thickness. Diamond markers represent measurements from microsample experiments. Results are also compared to Ti-6Al-4V measurements of ultimate tensile strength where the lath thickness was varied [18].

For the samples that failed by shear, the lowest strain to failure was most likely caused by large colonies that were misaligned to the tensile axis. This caused the formation of shear bands and yielding to occur at relatively low strains. The sooner the yielding and shear banding occurs, the sooner the voids nucleate and coalesce. Samples that showed a higher yield strength likely had either smaller colonies or colonies that were not as misaligned to the tensile axis within the gage section. This led to shear banding occurring at a higher value of strain within the sample, which led to the higher strain to failure.

For the samples that failed by ductile fracture, shear bands did not form, so the samples necked and fracture occurred due to void coalescence in the necked region. This explains the negative slope that was observed for both the weld samples as well as the base metal samples that failed by ductile fracture. This negative slope was also observed in the BM macroscale values obtained through different heat treatments. With an increase in strength, a decrease in ductility was found. This is different from what occurs with the base metal samples that failed by shear and supports the explanation that the microstructure of BM Ti-5111 strongly affected the failure mechanisms as well as the measured yield strength and strain to failure.

The strength of titanium alloys is controlled mainly by microstructural features such as the thickness of the α laths, the colony size, and the prior β grain size. Fig. 16 shows the ultimate tensile strength of Ti-5111 versus the α lath thickness for the base metal and weld samples compared to literature values for Ti-6Al-4V [18] and base metal Ti-5111 [24]. Both the literature values and the microsample measurements show similar trends; decreasing lath size causes an increase in strength. For the finer lath sizes, the weld samples showed similar values to the ultimate tensile strength at similar lath sizes found in the literature [18]. This result is expected, and differences that arise are due to other microstructural features such as the colony size or prior β grain size, as well as chemical composition.

5. Conclusions

The mechanical response of Ti5111 was examined using a custom microscale tension testing system that enables the observation and measurement of full field strains using DIC. The Ti-5111 material was examined across two grain morphologies, the base metal and the weld metal. The sizes of the microstructural features within the sample gage length were characterized and were found to strongly affect the mechanical responses on the micro scale. For the base metal, the measured strengths agreed with literature values at the macro scale. The average strain to failure of the base metal also agreed with macro-scale literature values, however the standard deviation of the strain to failure was high. This was found to be due to the size of the α colonies and orientation of α laths within the colony microstructure within the sample at the failure region, leading to two distinct failure modes. Small colonies with laths oriented more parallel to the tensile axis led to high ductility and ductile rupture, while laths inside large colonies that were oriented at an angle or perpendicular to the tensile axis led to lower ductility and shear failure. The yield strength, ultimate tensile strength, and strain to failure for the weld material were higher and showed significantly less variation than the base metal, due to refined grain size and more random orientation of the lath structures.

Acknowledgements

The authors would like to acknowledge the support of the Office of Naval Research (Contract number N00014-12-1-0415), and Naval

Surface Warfare Center Carderock Division. SEM images were obtained at the UMBC NanoImaging Center.

Data availability

The raw/processed data required to reproduce these findings cannot be shared at this time due to technical or time limitations.

References

- [1] S. Nimer, J. Wolk, M. Zupan, Location and orientation specific material property evaluation of friction stir welded Ti-5111: a microsample approach, *Adv. Eng. Mater.* 16 (2014) 452–458, <https://doi.org/10.1002/adem.201300427>.
- [2] S. Nimer, J. Wolk, M. Zupan, Local property characterization of friction stir welded Ti-5111: transverse orientation measurements, *Acta Mater.* 61 (2013) 3050–3059, <https://doi.org/10.1016/j.actamat.2013.01.065>.
- [3] C. Cheng, *Mechanical and Microstructural Characterization of Copper Microsamples After Cold Drawing*, University of Maryland Baltimore County, 2008.
- [4] D.A. LaVan, W.N. Sharpe, Tensile testing of microsamples, *Exp. Mech.* 39 (1999) 210–216, <https://doi.org/10.1007/BF02323554>.
- [5] S. Nimer, *Microscale Mechanical Experiments across Temperatures: System Development and Material Characterization*, Ph.D. Thesis, University of Maryland Baltimore County, 2016.
- [6] J. Wolk, *Microstructural Evolution in Friction Stir Welding of Ti-5111*, University of Maryland, College Park, 2010. <https://drum.lib.umd.edu/handle/1903/10409>.
- [7] M. Sutton, W. Wolters, W. Peters, W. Ranson, S. McNeill, Determination of displacements using an improved digital correlation method, *Image Vis. Comput.* 1 (3) (1983) 133–139, [https://doi.org/10.1016/0262-8856\(83\)90064-1](https://doi.org/10.1016/0262-8856(83)90064-1).
- [8] B. Pan, Recent progress in digital image correlation, *Exp. Mech.* 51 (7) (2011) 1223–1235, <https://doi.org/10.1007/s11340-010-9418-3>.
- [9] M.B. Gorji, D. Mohr, Micro-tension and micro-shear experiments to characterize stress-state dependent ductile fracture, *Acta Mater.* 131 (2017) 65–76, <https://doi.org/10.1016/j.actamat.2017.03.034>.
- [10] S. Venkatachalam, R. Banjare, H. Murthy, B.C. Rao, Mechanical testing of micro-specimens of Al6061-T6 using DIC for strain measurement, *Exp. Tech.* 43 (2019) 125–135, <https://doi.org/10.1007/s40799-018-0254-1>.
- [11] M. Aydin, X. Wu, K. Cetinkaya, M. Yasar, I. Kadi, Application of digital image correlation technique to Erichsen cupping test, *Engineering Science and Technology, an International Journal* 21 (2018) 760–768, <https://doi.org/10.1016/j.jestech.2018.06.004>.
- [12] B. Ahn, S.R. Nutt, Strain mapping of Al-Mg alloy with multi-scale grain structure using digital image correlation method, *Exp. Mech.* 50 (1) (2009) 117–123, <https://doi.org/10.1007/s11340-008-9211-8>.
- [13] A. Jung, J. Luksch, S. Diebels, F. Schäfer, C. Motz, In-situ and ex-situ micro-tensile testing of individual struts of Al foams and Ni/Al hybrid foams, *Mater. Des.* 153 (2018) 104–119, <https://doi.org/10.1016/j.matdes.2018.04.075>.
- [14] S.P. Mates, A.M. Forster, D. Hunston, R. Rhorer, R.K. Everett, K.E. Simmonds, A. Bagchi, Identifying the dynamic compressive stiffness of a prospective biomimetic elastomer by an inverse method, *J. Mech. Biomed. Mat* 14 (2012) 89–100, <https://doi.org/10.1016/j.jmbbm.2012.04.023>.
- [15] A. Campo, J. Soons, H. Heuten, G. Ennekens, I. Goovaerts, C. Vrints, P. Lava, J. Dirckx, Digital image correlation for full-field time-resolved assessment of arterial stiffness, *J. Biomed. Opt.* 19 (1) (2014) 016008, <https://doi.org/10.1117/1.JBO.19.1.016008>, January.
- [16] K. Gangwar, M. Ramulu, Friction stir welding of titanium alloys: a review, *Mater. Des.* 141 (2018) 230–255, <https://doi.org/10.1016/j.matdes.2017.12.033>, March.
- [17] ASTM E112-13, *Standard Test Methods for Determining Average Grain Size*, ASTM International, West Conshohocken, PA, 2013.
- [18] J. Tiley, T. Searles, E. Lee, S. Kar, R. Banerjee, J.C. Russ, H.L. Fraser, Quantification of microstructural features in alpha/beta titanium alloys, *Mater. Sci. Eng. A* 372 (2004) 191–198, <https://doi.org/10.1016/j.msea.2003.12.008>.
- [19] B. Pan, K. Qian, H. Xie, A. Asundi, Two-dimensional digital image correlation for in-plane displacement and strain measurement: a review, *Meas. Sci. Technol.* 20 (6) (2009), <https://doi.org/10.1088/0957-0233/20/6/062001>.
- [20] G. Lionello, L. Cristofolini, A practical approach to optimizing the preparation of speckle patterns for digital-image correlation, *Meas. Sci. Technol.* 25 (10) (2014), <https://doi.org/10.1088/0957-0233/25/10/107001>.
- [21] K.E. Knipling, R.W. Fonda, Microstructural evolution in Ti-5111 friction stir welds, *Metall. Mater. Trans. A* 42A (2011) 2312–2322, <https://doi.org/10.1007/s11661-011-0630-2>, August.
- [22] A.C. Robinson, *Optimizing Strength and Fracture Toughness of a Cast Titanium Alloy Through Heat Treatment and Microstructure Control*, Ph.D. Thesis, The Pennsylvania State University, 2007, <https://etda.libraries.psu.edu/catalog/7485>.
- [23] TIMETAL 5111. *TIMET.com*, 2015. http://www.timet.com/images/document/plateTIMETAL_5111.pdf.
- [24] A.C. Stauffer, E.J. Czyryca, D.A. Koss, The Influence of Processing on the Microstructure and Properties of the Titanium Alloy Ti-5111, *NSWCCD-61-TR-2004/16*, Sept. https://archive.org/details/DTIC_ADA430238, 2004.